Energy 112 (2016) 852–867

Contents lists available at ScienceDirect

Energy

journal homepage: www.elsevier.com/locate/energy

Design of oscillating-water-column wave energy converters with an application to self-powered sensor buoys

J.C.C. Henriques*, J.C.C. Portillo, L.M.C. Gato, R.P.F. Gomes, D.N. Ferreira, A.F.O. Falcão

LAETA, IDMEC, Instituto Superior Técnico, Universidade de Lisboa, Av. Rovisco Pais, 1049-001 Lisboa, Portugal

ARTICLE INFO

Article history:
Received 15 April 2016
Received in revised form
8 June 2016
Accepted 10 June 2016
Available online 5 August 2016

Keywords:
Wave energy converter
Oscillating water column
Oceanographic monitoring
Long term deployment

ABSTRACT

The quest for conquering the ocean and understanding its behaviour has been a challenge with increasing needs for innovation and technology investments in many areas of strategic value for the promotion, growth and competitiveness of the marine economy worldwide. Current oceanographic buoy systems are limited to low power levels and intermittency of data acquisition and transmission, among other aspects that need to be overcome to comply with new and more demanding applications. The development of marine activities requires more powerful and reliable data-acquisition systems to guarantee their future sustainability. This work presents a new systematic methodology for optimum design of wave energy converters. The methodology was applied to design two self-powered sensor buoys for long term monitoring based on the oscillating-water-column principle. The optimisation focussed on buoy hydrodynamic shape, sizing and selection of the turbine and the generator, as well as the control law of the generator electromagnetic torque. The performance was assessed through the use of the power matrix and a set of performance indicators. These performance indicators were defined to allow a simple comparison between different wave energy concepts. The results confirm the applicability of the designed buoys for a next generation of oceanographic monitoring systems.

1. Introduction

The overall demand for energy and associated services to meet social and economic development has become one of the most challenging problems of the global economy. The increase in the penetration of renewable energy in the energy mix has driven great efforts of R&D in the last decades, especially in the European Union (EU) [1,2], which has set up ambitious goals for the coming years.

The European Commission has established a series of initiatives based on the Marine Strategy Framework Directive for promoting the marine knowledge and seabed mapping. It has been estimated that high-quality marine data widely available in the EU would improve productivity by over €1 billion per year [3]. This sets urgent areas of development for better and long-lasting ocean observing systems. Reducing the costs for data acquisition is therefore a key priority in the EU. In this context, it is fundamental to develop cost-effective and multi-functional platforms, including sensors, to perform long-term monitoring and provide reliable *in situ* measurements of key parameters. The solution to this problem must take advantage of a new generation of technologies involving several domains of knowledge, such as: energy conversion and storage; data acquisition, pre-processing, storage and transmission; miniaturisation; communication; disposable non-pollutant technologies and standardisation.

The current capabilities of monitoring buoys are still quite limited by their energy source. That is, the existing sensor buoy power systems often include photovoltaic panels and batteries whose lifetime and power output are insufficient for modern applications [4]. Some sensor buoys are even designed to sink after exceeding the battery life because recharging is impractical or too costly, thus contributing to environmental and economical impacts [5].

The marine economy is driving ambitious projects for data-acquisition systems, which may involve sea-charging floating stations for autonomous underwater vehicles (AUVs) [6] and long-term deep ocean autonomous scientific observation systems [7]. Harnessing ocean wave energy with a reliable and self-sufficient system is an appealing concept for the electricity supply of on-

* Corresponding author.
E-mail addresses: joaochenriques@tecnico.ulisboa.pt (J.C.C. Henriques), juan.portillo@tecnico.ulisboa.pt (J.C.C. Portillo), luis.gato@tecnico.ulisboa.pt (L.M.C. Gato), ruigomes@tecnico.ulisboa.pt (R.P.F. Gomes), nevesferreira@tecnico.ulisboa.pt (D.N. Ferreira), antonio.falcao@tecnico.ulisboa.pt (A.F.O. Falcão).

http://dx.doi.org/10.1016/j.energy.2016.06.054
0360-5442/

Nomenclature

Romans

a	generator control law constant (19)
$\mathbf{A}_{ij}$	state matrix of the radiation R_{ij} state-space representation (6) [s^{-1}]
A_{ij}^{∞}	limiting value at infinite frequency of the added mass of body i as affected by body j motion [kg]
A_{ω}	wave amplitude (3) [m]
b	generator control law exponent (19)
$\mathbf{b}_{ij}$	input matrix of the radiation R_{ij} state-space representation (6) [m^{-1}]
$\mathbf{c}_{ij}$	output matrix of the radiation R_{ij} state-space representation (6) [N]
d_1	buoys outer diameter, see Figs. 7 and 11 [m]
d_2	buoys inner diameter, see Figs. 7 and 11 [m]
d	turbine rotor diameter [m]
E_{abs}	annual absorbed energy [kWh]
F_{di}	excitation force on body i (3) [N]
g	acceleration of gravity [m/s^2]
h	vertical length, see Figs. 7 and 11 [m]
H_s	significant wave height [m]
I	turbine/generator set moment of inertia [kg m^2]
m_i	mass of body i [kg]
$\dot{m}_{\text{turb}}$	turbine mass flow rate [kg/s]
p	absolute air chamber pressure [Pa]
p^*	dimensionless relative pressure (2) [−]
P_{abs}	absorbed power [W]
p_{at}	absolute atmospheric pressure [Pa]
P_{elect}	electrical power (21) [W]
$P_{\text{gen}}^{\text{em}}$	generator electromagnetic power (20) [W]
$P_{\text{gen}}^{\text{opt}}$	optimal generator power (19) [W]
$P_{\text{gen}}^{\text{rated}}$	generator rated power [W]
P_{turb}	turbine aerodynamic power (13) [W]
Q_{turb}	turbine volumetric flow rate [m^3/s]
R_{ij}	radiation damping forces on body i due to body j (6) [N]
S_1	floater water plane area [m^2]
S_2	OWC water plane area [m^2]
t	time [s]
t_{year}	annual operational time [h]
T_{e}	energy period [s]
$T_{\text{gen}}^{\text{em}}$	generator electromagnetic torque (23) [N m]
T_{turb}	turbine aerodynamic torque (17) [N m]
V_0	volume of air inside the chamber in calm water [m^3]
V_{c}	instantaneous air chamber volume [m^3]
v_i	velocity of body i [m/s]
$\mathbf{x}$	system state (24)
x_i	vertical position body i [m]
$\mathbf{X}_1$	Fast Fourier Transform of $\mathbf{x}_1$ [m s]
$\mathbf{y}_{ij}$	radiation state R_{ij} (5) [−]

Greek symbols

β	constant (10) [−]
γ	specific heat ratio of air, C_p/C_v [−]
Γ_i	excitation force of body i per unit wave height [N/m]
Δt	time interval used to discretize the ODE system (24) [s]
η_{turb}	turbine efficiency (14) [−]
η_{gen}	generator efficiency, Fig. 6b unit wave amplitude (3) [−]
κ	polytropic exponent (18) [−]
Λ_{gen}	generator load (22) [−]
Π	turbine dimensionless power (13) [−]
Π_d	displacement per unit of significant wave height (33) [−]
Π_{EV}	annual absorbed energy per unit of submerged volume (32) [kWh/m^3]
Π_F	absorbed power per unit of linear velocity of the PTO (29) [N]
ϱ	air density [kg/m^3]
ϱ_{at}	air density at atmospheric conditions [kg/m^3]
ϱ_{in}	stagnation air density at turbine inlet (15) [kg/m^3]
ϱ_{w}	water density [kg/m^3]
Φ	turbine dimensionless flow rate (12) [−]
ϕ_i	phase of body i response (3) [rad]
Ψ	turbine dimensionless pressure head (11) [−]
ω	wave frequency (3) [rad/s]
Ω	turbine/generator set rotational speed [rad/s]

Superscripts

*	dimensionless quantity
em	electromagnetic quantity
opt	optimal value
rated	rated quantity
rms	root-mean-square
T	transpose operator

Subscripts

1	buoy, denoted as body 1 in (1)
2	weightless rigid piston, denoted as body 2 in (1)
at	atmospheric quantity
c	chamber
elect	electrical quantity
gen	generator quantity
in	turbine inlet conditions
max	maximum value
n	sea state
turb	turbine quantity

board sensors. In particular, the recent development of self-powered buoys equipped with data acquisition sensors suggests a novel way to use moored buoys to extract energy from waves, while providing continuous real-time data measurements for ocean monitoring. The MBARI's Wave-Power Buoy is one of the prototypes designed to fulfil such roles [8,9].

The concept of harvesting wave energy for powering small buoys is not new. Yoshio Masuda (1925–2009) was the first to develop navigation buoys powered by wave energy [10]. The device is basically a floater rigidly pierced by a vertical tube, see Fig. 1a. The upper part, above the water line, forms an air chamber open to the atmosphere through a duct where an air turbine is installed. Wave action alternately compresses and decompresses the trapped air which forces air to flow through the turbine [11]. Masuda's systems were later known as floating oscillating-water-column devices (OWCs). The original Masuda's buoys used conventional unidirectional turbines instead of self-rectifying (bidirectional) air turbines. This required rectifying valves which affected the energy conversion efficiency (see Fig. 1b). Due to their inherent simplicity and reliability, more than one thousand of these navigation buoys were deployed in Japan, China and USA [10,12]. Remarkably, several of these buoys were fully operational for more than three decades.

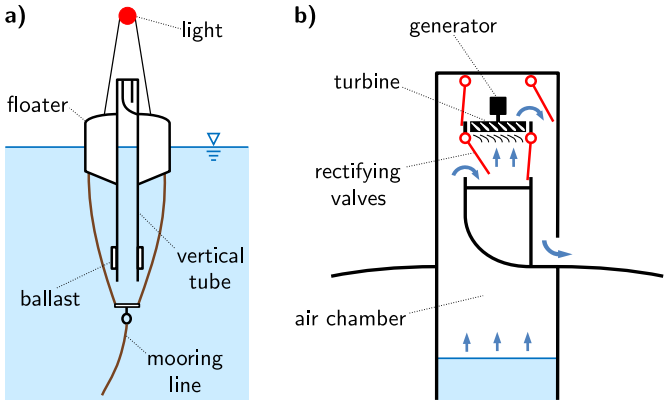

Fig. 1. a) Yoshio Masuda's navigation buoy based on the OWC principle. b) Detail of the turbine and the rectifying valves of the PTO system under exhalation conditions.

Fig. 2 shows three basic types of OWC wave energy converters (WECs). The first one, see Fig. 2a, is of a fixed type and is suitable to be incorporated in traditional breakwaters, generally of reinforced concrete structure type, such as the breakwater of Mutriku port [13], in the Basque country. Remarkably, one of the first fixed OWC was installed in 1999 at the island of Pico, in the Azores archipelago, is still operational [14]. A variant of this WEC is the U-shaped OWC geometry proposed by Bocotti [15] which consists of an additional vertical duct at the wave-beaten side, see wall represented by a broken line in Fig. 2a; a large number of these devices are being installed at a breakwater under construction at the port of Civitavecchia, Italy [16]. The second type is a spar-buoy OWC, an optimised version of Masuda's buoy, see Fig. 2b. The third type has been named coaxial-duct OWC and was originally proposed by Takahashi Takashi [17] in 1980, see Fig. 2c. This axisymmetric floating device is formed by two coaxial tubes. The inner tube is partially submerged, connected at the upper part to the atmosphere through an air turbine and at the bottom part to the water duct formed by the coaxial tubes. A recent review about the OWC technology and air turbines can be found in Ref. [18].

The power take-off (PTO) systems of OWCs are generally equipped with self-rectifying air turbines. In this configuration the only moving part of a floating OWC WEC is the rotor of an air turbine directly driving a conventional electrical generator [19]. The axial-flow Wells turbine, invented in the mid-1970s, is the best known self-rectifying turbine, Fig. 3a. It is characterized by its mechanical simplicity and by limitations in its aerodynamic efficiency [20]. The more recent biradial impulse turbine, that is adopted in this study, is a more efficient self-rectifying turbine that overcomes some of the limitations of the Wells turbine [11,21,22].

The OWC-based WECs have been extensively studied for large scale wave resource exploitation and some prototypes were deployed into the ocean [23,24]. However, the new OWC WECs for oceanographic applications have specific design constraints since a simple geometric scaling results in a low efficiency device that fails to achieve the desirable resonance conditions in ocean waves.

One of the main characteristics of wave energy is its intermittency. Monitoring buoys based on this type of energy supply will require complementary power sources such as photovoltaic panels [25] and or novel systems based on thermoelectric materials [26,27]. Nevertheless, the intermittency of these energy sources will require battery storage to complement and smoothen the power supply required by the monitoring instrumentation. The integration of these sub-systems in a monitoring buoy is out of the scope of this paper.

The present paper is focused on the detailed design of two OWC sensor buoys for oceanographic applications, namely the hydrodynamic optimisation of the buoy and the PTO sizing and selection. The performance assessment was carried out considering the wave climate characteristic of the western coast of Portugal. The proposed methodology can also be used for OWC devices aiming for large scale wave energy exploitation.

The contributions of the present work are:

- an improved numerical model of the air chamber pressure considering a polytropic expansion/compression based on the instantaneous turbine efficiency;
- evaluation of the combined efficiencies of the turbine and the generator in the electrical power output;

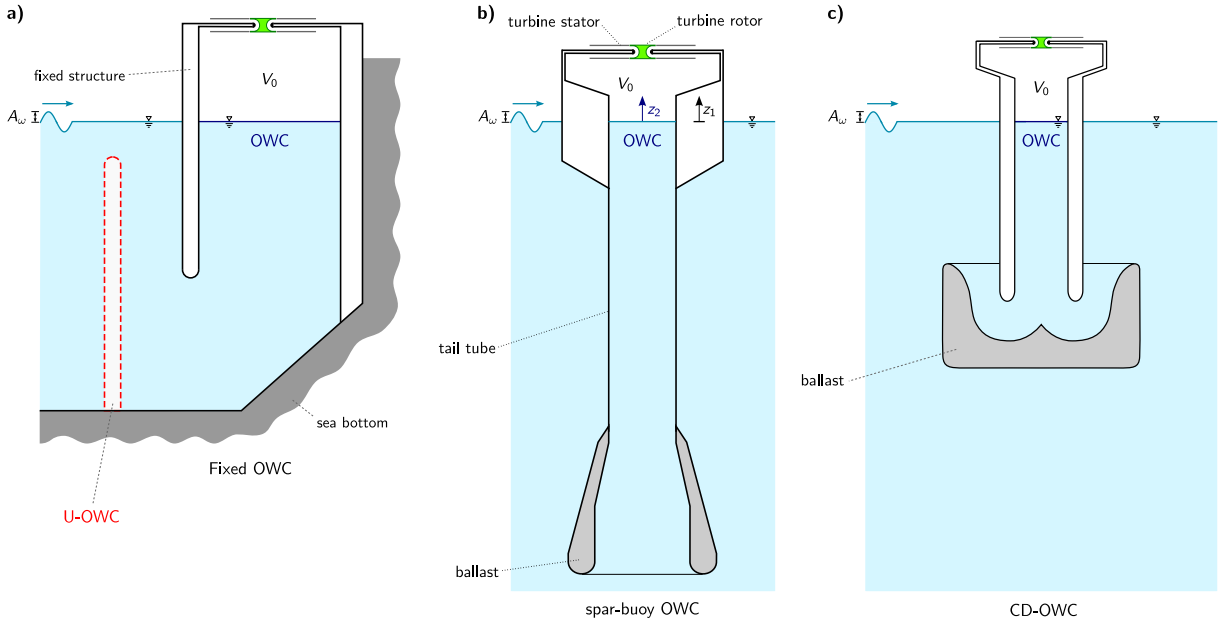

Fig. 2. a) Cross section of a fixed OWC converter. b) Cross section view of the oceanographic spar-buoy OWC. c) Cross section view of the oceanographic coaxial-duct OWC.

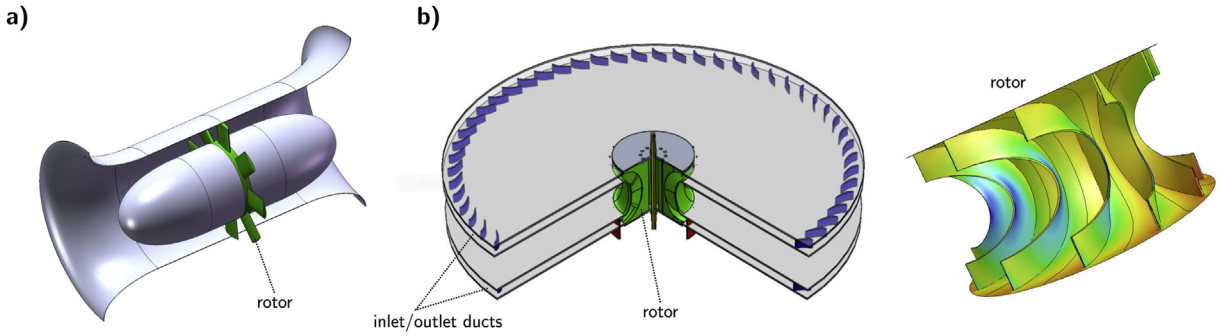

Fig. 3. a) The Wells turbine and b) the biradial turbine.

- a systematic representation of the life-cycle of a wave energy project;
- a detailed design methodology for oscillating water column wave energy converters with an application to two wave-powered oceanographic sensor buoys;
- a simple and effective methodology for the optimal choice of the turbine/generator set including the generator control law;
- definition of three new performance indicators to complement the set proposed by Babarit et al. [28].

The structure of the paper is as follows. Section 2 introduces a general overview of a wave energy project. Section 3 describes the numerical model of two different floating OWC technologies. The design process and the definition of performance indicators used to compare the devices are presented in Section 4. Results are discussed in Section 5. Conclusions are drawn in Section 6.

2. Overview of a wave energy project

The project development process of a wave energy system may be outlined, in general, as in Fig. 4. Iterative loops and complex interdependencies have been neglected for ease of reading. The process might be split into two main sub-processes: design and implementation.

The overall **design process** comprises three phases:

- A **preliminary design** that starts with the definition of WEC and PTO concept(s), definition of the numerical model(s), site data gathering and analysis up to the validation of the model(s). The preliminary design should include a performance assessment to determine if the basic conception might be of interest for further development. The evaluation is done based on previously defined requirements.
- A **detailed design** accomplished by an optimisation phase followed by a performance assessment. The optimal hydrodynamic shape of the device should maximize the time-averaged energy absorption under realistic system constraints. The PTO system is also to be designed at this phase as well as the control strategy and all related parameters.
- **Model testing** at small, medium and/or large scale to evaluate the performance of the wave energy concept and tune the system components to achieve maximum efficiency and reliability.

It is important to remark that the detailed design and model testing is a time-consuming and expensive iterative process towards a successful commercial product.

During these phases, there must be a design process assessment that involves key performance indicators to evaluate the design(s) from different perspectives, in order to aid in the decision-making process of selecting options and deciding to undertake further and more expensive stages of development. It is obvious that not all technologies will follow all these sub-processes, if they are not expected to fulfil all the requirements. In such a situation, they can be discarded at any time, which probably will open the door to a new series of technological solutions. This is the reason why it is important to assess the design options at different levels and phases. The assessment should involve different perspectives to get a complete picture of the potential feasibility of a wave energy project.

The **implementation process** involves the construction, deployment, operation & maintenance, and final dismantling when the life time of the project comes to its end. It follows the traditional decomposition in sub-processes as commonly performed in most project developments, see for example [29]. All these sub-processes should be followed by constant monitoring and control, as normally it is done in any other project development and organizational processes. The implementation process is out of the scope of the present paper.

The proposed project development process is general and can be applied to different kinds of wave energy conversion technologies. It was not restricted to any specific wave energy converter or PTO system. The design process consists of a series of sub-processes, activities or tasks that are common to the development of wave energy technologies. Some advancements have been done separately and in various ways by wave energy developers, such as those found in Refs. [19,30–34].

To the authors knowledge, no overall procedure for the development of a wave energy project can be found in the literature. In Refs. [30], a methodology is presented for optimizing the SEAREV WEC in terms of hydrodynamic, mechanical, electrical and control interdependencies. Gomes et al. [19], presented a methodology for optimizing a large size spar-buoy OWC, which has been used in this work as part of the overall process. Furthermore, [31] focuses on the development and validation of a numerical model for the WaveRoller, reflecting the early stages of the design of a WEC. Regarding the Pelamis, which was one of the few technologies that reached an advanced stage of development and testing, [32] describes the path used without establishing a real methodology for the life-cycle of a project. In Ref. [33], a feasibility analysis study is presented for the Pelamis, using real data, as well as an assessment based on economical performance indicators. Results for an open-sea prototype testing of the WaveDragon WEC at 1:5 scale can be found in Ref. [34].

All these cases exemplify practices undertaken in different WEC but are just a part of the global process. Experiences and best practices have been integrated as a whole and systematized in the presented process for the life-cycle of wave energy projects. In general, it has been observed that information and knowledge have

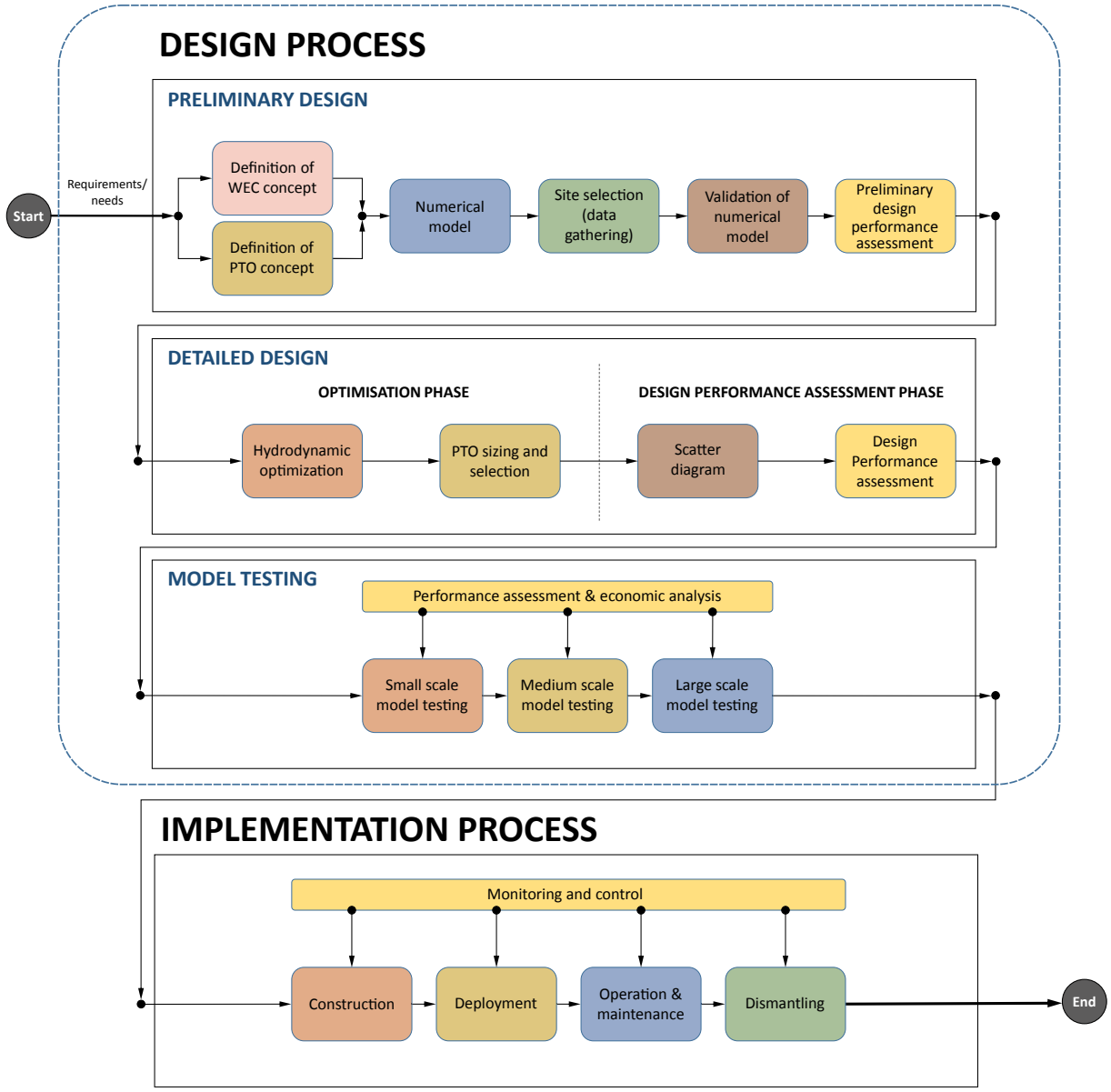

Fig. 4. Schematic representation of the life cycle of a wave energy project.

been presented dispersed and without integration. There is evidence that developers have done something based on the degree of the technology development level of their systems, but not global overviews have been reported in a systematic and comprehensive way.

Wave energy is still at an early stage of development and there is no direct experience of implementing real commercial projects. Technological readiness levels (TRLs) are used to describe the state of development of engineering projects [36]. Weber [35] proposed a complementary metric of technological performance levels (TPLs) that aims to characterize the technical and economic performance of WECs. The representation of TRL and TPL in a two-dimensional matrix allows to evaluate and compare the development paths of different technologies, and highlights the need to design strategies to follow paths with higher TPLs at lower TRLs [35], see Fig. 5.

The design and implementation process described in the present work can be applied to any path followed by a WEC project along the TRL-TPL-matrix. The spar-buoy OWC and the biradial turbine have been experimentally tested and validated at different scales [37–40]. Therefore, the spar-buoy OWC is in TRL-4 and TPL-5 considering the niche market of self-powered sensor buoys. The coaxial-ducted OWC is in a much lower development stage, about TRL-2 and TPL-2, see Fig. 5.

3. Numerical modelling

3.1. Spar-buoy OWC model

The oceanographic spar-buoy OWC was modelled as a two-body system. The coupling between the two bodies is due to PTO forces and to the forces associated to the diffracted and radiated wave fields. The numerical model was based on linear wave theory, coupled with a fully non-linear compressibility formulation for the air in the pneumatic chamber. This, in conjunction with the non-linear flow rate versus pressure drop characteristic of the biradial turbine, resulted in a non-linear system, and so a time-domain

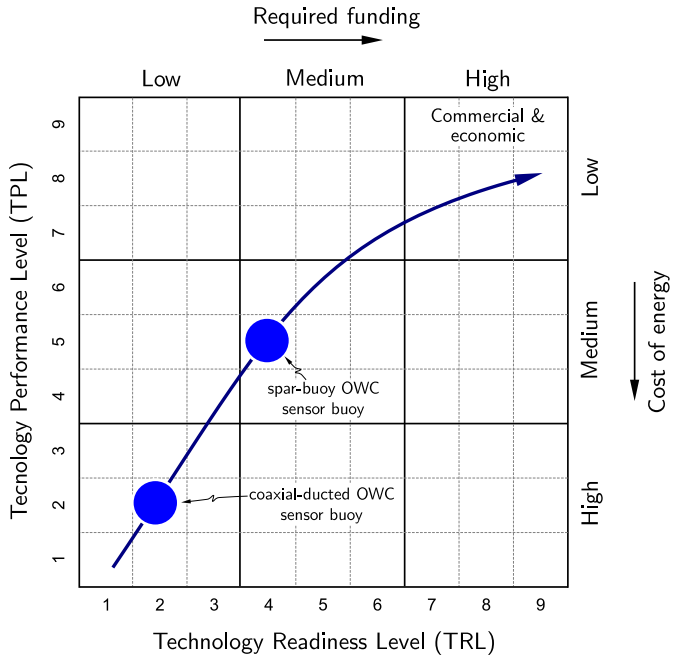

Fig. 5. The TRL and TPL of the spar-buoy OWC and the coaxial-duct OWC for oceanographic monitoring applications (Adapted from Ref. [35]).

approach was needed. The non-dimensional performance curves of the biradial turbine were obtained from model testing [37].

The spar-buoy (floater and tail tube) was named here as body 1, see Fig. 2b. The air-water interface was modelled as an imaginary weightless rigid piston denoted as body 2. In the present case, the weightless rigid piston should be a good approximation since the OWC diameter is much smaller than the wave length.

Let x_i be the coordinates of body i for the heave motion, with $x_i = 0$ at equilibrium position and the x_i-axes pointing upwards. The equations of motion for the two-body system are [38].

$$\left(m_1 + A_{11}^{\infty}\right)\ddot{x}_1 + \varrho_w g S_1\, x_1 + A_{12}^{\infty}\,\ddot{x}_2 - p_{\mathrm{at}}\, S_2\, p^* = F_{\mathrm{d},1} - R_{11} - R_{12}, \tag{1a}$$

$$\left(m_2 + A_{22}^{\infty}\right)\ddot{x}_2 + \varrho_w g S_2\, x_2 + A_{21}^{\infty}\,\ddot{x}_1 + p_{\mathrm{at}}\, S_2\, p^* = F_{\mathrm{d},2} - R_{22} - R_{21}. \tag{1b}$$

Here, the dots denote time derivatives, g is the acceleration of gravity, ϱ_w is water density, S_i is the annular cross sectional area of body i, m_i is the mass of body i, A_{ij}^{∞} represents the limiting value at infinite frequency of the added mass of body i as affected by the motion of body j. The dimensionless relative pressure oscillation inside the chamber is defined as

$$p^* = \frac{p}{p_{\mathrm{at}}} - 1, \tag{2}$$

where p_{at} is the atmospheric pressure, and p is the instantaneous pressure inside the air chamber.

Since we were assuming linear water wave theory, the resulting diffraction force was obtained as a superposition of N angular frequency components, ω_m,

$$F_{\mathrm{d},i} = \sum_{m=1}^{N} \Gamma_i(\omega_m)\, A_m \cos\left(\omega_m t + \phi_{i,m} + \phi_r\right), \tag{3}$$

where $\Gamma(\omega_m)$ is the excitation force coefficient, A_m is the frequency-dependent wave amplitude, $\phi_{i,\,m}$ is the phase response of body i at the angular frequency ω_m and ϕ_r is a random phase; see Refs. [41,42] for details.

The radiation force was defined as $A_{11}^{\infty}\ddot{x}_1 + R_{ij}$ where

$$R_{ij} = \int_0^t K_{ij}(t-s)\,\dot{x}_j(s)\,\mathrm{d}s. \tag{4}$$

The added masses, A_{ij}^{∞}, the excitation force coefficients, Γ_i, the phase responses, ϕ_i, and the kernel K_{ij} were computed using the WAMIT software package [43]. This software uses a Boundary Integral Equation Method to compute this coefficients as function os the wave frequency, as described in Refs. [43,44].

The convolution integrals appearing in R_{ij} were approximated by a linear state-space model obtained with a system identification procedure [45].

$$\dot{\mathbf{y}}_{ij} = \mathbf{A}_{ij}\mathbf{y}_{ij} + \mathbf{b}_{ij}\dot{x}_j, \tag{5}$$

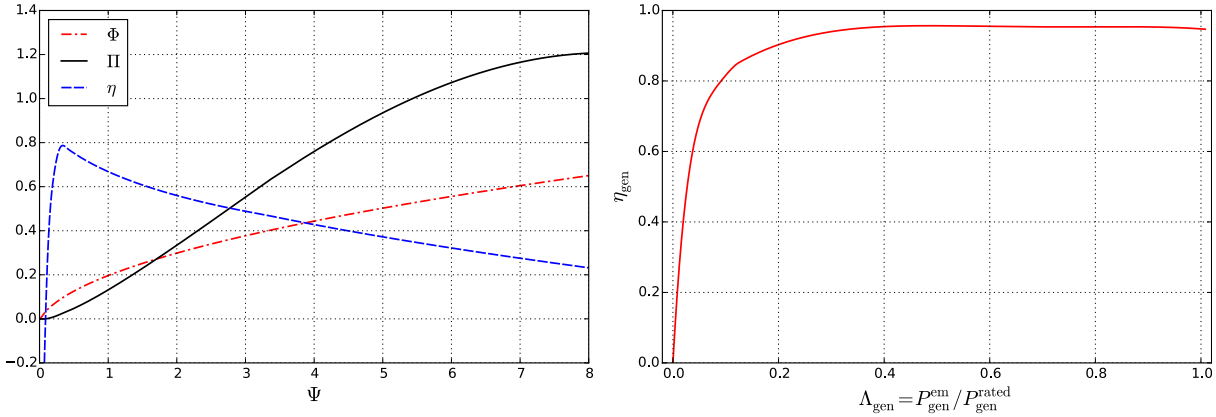

Fig. 6. a) Dimensionless flow rate, Φ, dimensionless power coefficient, Π, and efficiency, η, as functions of the dimensionless pressure head, Ψ, for the biradial turbine used in the numerical simulations, based on [37]. b) Generator efficiency curve taken from Ref. [51].

$$R_{ij} = \mathbf{c}_{ij}^T \mathbf{y}_{ij}, \tag{6}$$

where $\mathbf{y}_{ij} \in \mathbb{R}^{p\times 1}$ are auxiliary variables used in the computation of R_{ij}. The matrices $\mathbf{A}_{ij} \in \mathbb{R}^{p\times p}$, $\mathbf{b}_{ij} \in \mathbb{R}^{p}$ and $\mathbf{c}_{ij} \in \mathbb{R}^{p}$ were obtained using a Matlab toolbox for parametric identification of radiation-force models of ships and offshore structures, see Ref. [46]. Here, the same degree of approximation p for all the radiation terms were used.

3.2. Air chamber model

The pressure in the air chamber is related to the mass flow rate of air through the turbine, $\dot{m}_{\text{turb}}$, (positive for outward flow) which is given by

$$-\dot{m}_{\text{turb}} = \varrho \dot{V}_{\text{c}} + V_{\text{c}}\, \dot{\varrho}, \tag{7}$$

where ϱ is the air density, $V_{\text{c}} = V + S_2(x_1 - x_2)$ is the instantaneous volume of air inside the chamber and V_0 is the volume at hydrostatic conditions. Assuming that air behaves as a perfect gas, the compression/expansion of the air in the chamber was modelled as a polytropic process

$$\frac{p}{\varrho^{\kappa}} = \frac{p_{\text{at}}}{\varrho_{\text{at}}^{\kappa}}, \tag{8}$$

where κ is the polytropic index related to the turbine efficiency, see Section 3.3. Equations (7) and (8) yield

$$\dot{p}^* = -\kappa(p^* + 1)\frac{\dot{V}_{\text{c}}}{V_{\text{c}}} - \kappa(p^* + 1)^{\beta}\frac{\dot{m}_{\text{turb}}}{\varrho_{\text{at}} V_{\text{c}}}, \tag{9}$$

with

$$\beta = \frac{\kappa - 1}{\kappa}, \tag{10}$$

see also [38,47,48].

3.3. The turbine/generator set model

The performance characteristics of the turbine are usually presented in dimensionless form, where

$$\Psi = \frac{p_{\text{at}}\, p^*}{\varrho_{\text{in}}\, \Omega^2\, d^2}, \tag{11}$$

$$\Phi = \frac{\dot{m}_{\text{turb}}}{\varrho_{\text{in}}\, \Omega\, d^3}, \tag{12}$$

$$\Pi = \frac{P_{\text{turb}}}{\varrho_{\text{in}}\, \Omega^3\, d^5}, \tag{13}$$

$$\eta_{\text{turb}} = \frac{\Pi}{\Phi\, \Psi}, \tag{14}$$

are the dimensionless pressure head, the dimensionless flow rate, the dimensionless power coefficient and turbine efficiency, see Refs. [49,50]. In Eqs. (11)–(13), Ω is the turbine rotational speed (in radians per unit time) and d is the turbine rotor diameter. The reference density ϱ_{in} is defined in stagnation conditions at the turbine entrance. Consequently, reference density is function of the pressure difference between the air chamber and the atmosphere and was computed as

$$\varrho_{\text{in}} = \varrho_{\text{at}}\, \max(\, p^* + 1,\ 1\,)^{1/\kappa}. \tag{15}$$

Neglecting the effects of the variations in Reynolds number (since the Reynolds number is in general large enough for that) and Mach number (see Refs. [49,50]), the dimensionless variables Φ, Π and η_{turb} can be plotted as simple curves as function of Ψ, as shown in Fig. 6.

The dynamics of the turbine/generator set was described by

$$I\, \dot{\Omega} = T_{\text{turb}} - T_{\text{gen}}^{\text{em}}, \tag{16}$$

where T_{turb} and $T_{\text{gen}}^{\text{em}}$ are the instantaneous turbine aerodynamic torque and the instantaneous generator electromagnetic torque, the latter being imposed by the rotational speed control law. The turbine aerodynamic torque was computed from Equations. (13) and (14)

$$T_{\text{turb}} = \varrho_{\text{in}}\, \Omega^2 d^5\, \eta_{\text{turb}} \Phi \Psi. \tag{17}$$

The polytropic exponent κ was related to the turbine polytropic efficiency (or small-stage efficiency) by (see Ref. [49])

$$\kappa = \frac{1}{1 - \frac{\gamma - 1}{\gamma}\eta_{\text{turb}}}, \tag{18}$$

where $\gamma = 1.4$ is the specific heat ratio for air. For outflow conditions, $p^* > 0$, $\varrho_{\text{in}} = \varrho$ and the values of η_{turb}, Ψ, and κ are determined iteratively since they form a non-linear system of equations.

3.4. The generator control law

The air turbine type and size, the control of the turbine rotational speed and the rated power of the electrical equipment strongly affect the power performance of the device [52,53]. In Refs. [53], different self-rectifying biradial turbine rotor diameters were simulated considering a set of sea states. In none of the cases the tip speed exceeded 120 m/s, which was considered by the authors acceptable in terms of Mach number and centrifugal stresses.

The PTO system for the oceanographic buoys under analysis consists of a biradial turbine and a generator. Eq. (13) shows that the turbine output power should be proportional to Ω^3 if the time-averaged turbine aerodynamic efficiency is to be maximized. In practice, if the coupling between the turbine aerodynamics and the spar-buoy OWC hydrodynamics is taken into account, we can use a relation of the type [54].

$$P_{\text{gen}}^{\text{opt}} = a\, \Omega^b. \tag{19}$$

In a previous study [54], it was found that exponent b should be about 3, for maximum overall (OWC plus turbine) time-averaged efficiency, *i.e.*, if the power output of the turbine is to be maximized. Furthermore, in the same study, it was found that the optimal time averaged turbine power versus rotational speed for each sea state follows approximately a straight line in a log-log scale.

To avoid overpowering the generator, it was adopted the following control law

$$P_{\text{gen}}^{\text{em}} = \min\left(P_{\text{gen}}^{\text{opt}}, P_{\text{gen}}^{\text{rated}}\right), \tag{20}$$

where $P_{\text{gen}}^{\text{rated}}$ is the rated (maximum allowed) power of the generator.

The generator electrical power output was estimated using

$$P_{\text{elect}} = \eta_{\text{gen}}(\Lambda_{\text{gen}})\, P_{\text{gen}}^{\text{em}}, \tag{21}$$

where the generator efficiency η_{gen} has been taken from Refs. [51], see Fig. 6b, as function of the load

$$\Lambda_{\text{gen}} = \frac{P_{\text{gen}}^{\text{em}}}{P_{\text{gen}}^{\text{rated}}}. \tag{22}$$

Therefore, the instantaneous generator electromagnetic torque follows the relation

$$T_{\text{gen}}^{\text{em}} = P_{\text{gen}}^{\text{em}}\, \Omega^{-1}. \tag{23}$$

Turbine runaway speed, as a result from zero generator torque due to electrical failure, is discussed in Section 5.

3.5. Global system of ODEs

The spar-buoy OWC was modelled by a system of first-order differential equations

$$\dot{\mathbf{z}} = \mathbf{F}(t, \mathbf{z}). \tag{24}$$

The state vector was defined by

$$\mathbf{z} = \left(v_1 \;\; v_2 \;\; x_1 \;\; x_2 \;\; p^* \;\; \Omega \;\; \overline{P}_{\text{turb}} \;\; \overline{P}_{\text{elect}} \;\; \mathbf{y}_{11}^T \;\; \mathbf{y}_{12}^T \;\; \mathbf{y}_{21}^T \;\; \mathbf{y}_{22}^T \right)^T, \tag{25}$$

where $\overline{P}_{\text{turb}}$ and $\overline{P}_{\text{elect}}$ are the time-averaged turbine and electrical power outputs. Using (25), the right-hand side of (24) becomes

$$\mathbf{F}(t, \mathbf{z}) = \begin{pmatrix} M_2^* \mathscr{F}_1 - A_{12}^* \mathscr{F}_2 \\ M_1^* \mathscr{F}_2 - A_{21}^* \mathscr{F}_1 \\ v_1 \\ v_2 \\ -\kappa(p^*+1)\dfrac{\dot{V}_c}{V_c} - \kappa(p^*+1)^{\beta}\dfrac{\dot{m}_{\text{turb}}}{\varrho_{\text{at}} V_c} \\ I^{-1}\left(T_{\text{turb}} - T_{\text{gen}}^{\text{em}}\right) \\ P_{\text{turb}}\, T_f^{-1} \\ P_{\text{elect}}\, T_f^{-1} \\ \mathbf{A}_{11}\mathbf{y}_{11} + \mathbf{b}_{11} v_1 \\ \mathbf{A}_{12}\mathbf{y}_{12} + \mathbf{b}_{12} v_2 \\ \mathbf{A}_{21}\mathbf{y}_{21} + \mathbf{b}_{21} v_1 \\ \mathbf{A}_{22}\mathbf{y}_{22} + \mathbf{b}_{22} v_2 \end{pmatrix}, \tag{26}$$

where $\dot{x}_1 = v_1$, $\dot{x}_2 = v_2$, $\mathscr{D} = (m_1 m_2 - A_{12}^{\infty} A_{21}^{\infty})^{-1}$, $M_i^* = \mathscr{D}(m_i + A_{ii}^{\infty})$, $A_{ij}^* = \mathscr{D} A_{ij}^{\infty}$, and

$$\mathscr{F}_1 = -\varrho_w g S_1\, x_1 + S_2\, p_{\text{at}}\, p^* + F_{d1} - \mathbf{c}_{11}^T \mathbf{y}_{11} - \mathbf{c}_{12}^T \mathbf{y}_{12}, \tag{27a}$$

$$\mathscr{F}_2 = -\varrho_w g S_2\, z_2 - S_2\, p_{\text{at}}\, p^* + F_{d2} - \mathbf{c}_{21}^T \mathbf{y}_{21} - \mathbf{c}_{22}^T \mathbf{y}_{22}. \tag{27b}$$

A Runge-Kutta forth-order time integration was used to solve (24) with the initial conditions

$$\mathbf{z}_0 = \left(0 \;\; 0 \;\; 0 \;\; 0 \;\; 0 \;\; \Omega_0 \;\; 0 \;\; 0 \;\; 0_p \;\; 0_p \;\; 0_p \;\; 0_p \right)^T, \tag{28}$$

where 0_p denotes a row vector of zeros with dimension p. All the numerical results were obtained considering an integration period of 1 h and with a time step of 0.1 s.

3.6. Coaxial-duct OWC model

The coaxial-duct OWC device is depicted in Fig. 2c. This system was modelled as a two-body system like the spar-buoy OWC. The PTO system is also a biradial air turbine that is driven by the pressure difference between the air chamber and the atmosphere. The same mathematical approach and numerical tools were used.

4. Detailed design

4.1. Optimisation phase

The optimisation phase of OWC WECs was divided into two parts: hydrodynamic optimisation of the buoys and PTO selection and sizing. For design purposes there is a fundamental difference between the sizing of the turbine and the generator. Only off-the-shelf electrical generators were considered due to the high availability of these components. This is not the case of air turbines, since they must be manufactured for this specific application. The overall methodology can be summarized as follows.

- Hydrodynamic optimisation
  - Optimize the buoy geometry using a stochastic hydrodynamic approach based on a frequency domain analysis in which a linear flow-rate-versus-pressure-head characteristic is assumed for the turbine. Full details of this design can be found in Ref. [19].
- PTO sizing and selection
  - Define a discrete set of turbine diameters denoted as $\mathscr{D}$.
  - For each $d \in \mathscr{D}$, compute the time-averaged turbine output power, $\overline{P}_{\text{turb}}$, as function of rotational speed, Ω, for each sea state, n, of the deployment site, see Table 1. A constant rotational speed model, $I\dot{\Omega} = 0$, is assumed over the time-averaged integration.
  - For each $d \in \mathscr{D}$, compute the set of rotational speeds, $\Omega_{\text{opt},n}$, that maximize the time-averaged turbine power output, $\overline{P}_{\text{turb}}$, for each sea state, n, of the deployment site.
  - For each $d \in \mathscr{D}$, compute the constants a and b of (19) that best fit the set of rotational speeds $\Omega_{\text{opt},n}$, see Refs. [53,54] for further details.
  - From a set of commercially available generators, select the one that better matches the time-averaged power output and the typical rotational speed of the turbine for the wave climate of the deployment site.
  - Check if the generator is able to withstand the turbine runaway speed in case of failure of the electrical components resulting in zero electromagnetic torque, $T_{\text{gen}}^{\text{em}} = 0$. Typically, this specification may require simple modifications to the shaft and bearings of the standard generator.

In this design process the effect of the turbine/generator inertia was not considered. As will be shown, the inertia has negligible effect on the buoys' performance within the range of practical interest. If required, the analysis of the effect of the inertia on the system performance is straightforward to implement in the presented methodology.

4.2. Design performance assessment phase

The assessment of renewable energy technologies is in general a multi-criteria decision-making process, which involves various dimensions associated to sustainability issues and human activities

Table 1
Characteristic wave climate off the western coast of Portugal. Each sea state, n, of the wave climate is defined by the significant wave height, H_s, energy period, T_e, and probability of occurrence, P_o [19].

n	H_s [m]	T_e [s]	P_o [%]
1	1.10	5.49	7.04
2	1.18	6.50	12.35
3	1.23	7.75	8.17
4	1.88	6.33	11.57
5	1.96	7.97	20.66
6	2.07	9.75	8.61
7	2.14	11.58	0.59
8	3.06	8.03	9.41
9	3.18	9.93	10.07
10	3.29	11.80	2.57
11	4.75	9.84	4.72
12	4.91	12.03	2.81
13	6.99	11.69	1.01
14	8.17	13.91	0.39

[55]. In this sense, these dimensions can be classified as technical, economical, environmental and social.

On the one hand, the technical dimension criterion evaluates the energy production capacity, the technological maturity, reliability and safety, whereas the economical dimension deals with the investment costs, operation and maintenance (O&M) costs, service life and the payback period. On the other hand, the environmental dimension criterion assesses the impact on ecosystems. In general, a distinction is made regarding the emissions of CO_2 which are an important measure when dealing with energy systems. The social dimension evaluates the benefits and acceptability [55].

Unlike in the wind energy industry, a wide variety of technologies are available for wave energy conversion, without any clear winner or preferred technology among the developers [23]. Currently, there is no widely accepted set of performance indicators to compare different WECs, apart from the mean power output or annual absorbed energy. Usually, the best way to compare different designs is to compute the scatter diagrams of turbine power output and/or electrical power output. This approach makes it difficult to get a fair comparison among WECs technologies and, even more, to select the proper one for a certain application.

The social and environmental impacts should be no less important in the assessment of WEC technologies. However, in the cases analysed here, there are no significant differences in this respect between the two proposed technologies. Consequently, these impacts will not be considered in this work. Furthermore, from the technical and economical perspectives, the technological maturity, safety, reliability, service life and O&M costs are very similar for the two WEC technologies presented. Based on this, only indicators associated to the energy production capacity and investment costs will be assessed.

A recent study by Babarit et al. [28] presented a set of performance measures that can be related to costs and energy production. In that study, fifteen different WEC devices for large power production were compared. Here, a similar procedure was used to perform a comparison between the WECs studied for oceanographic applications.

The power output is an important parameter to estimate the average cost of energy (€/kWh) in the case of large-scale energy production [28]. This indicator is estimated as the summation of the power output in each characteristic sea state times its probability of occurrence, and represents a decisive factor for running or not a project. The cost estimation at an early stage of development of WECs is an unreliable task and out of the scope of this work. There are currently a lot of uncertainties regarding the evolution of fabrication, installation, O&M and decommissioning costs. It is expected, as expressed in Refs. [28], that the performance indicators are good cost estimators.

In the present work, three new performance indicators are proposed to complement the initial set described by Babarit et al.

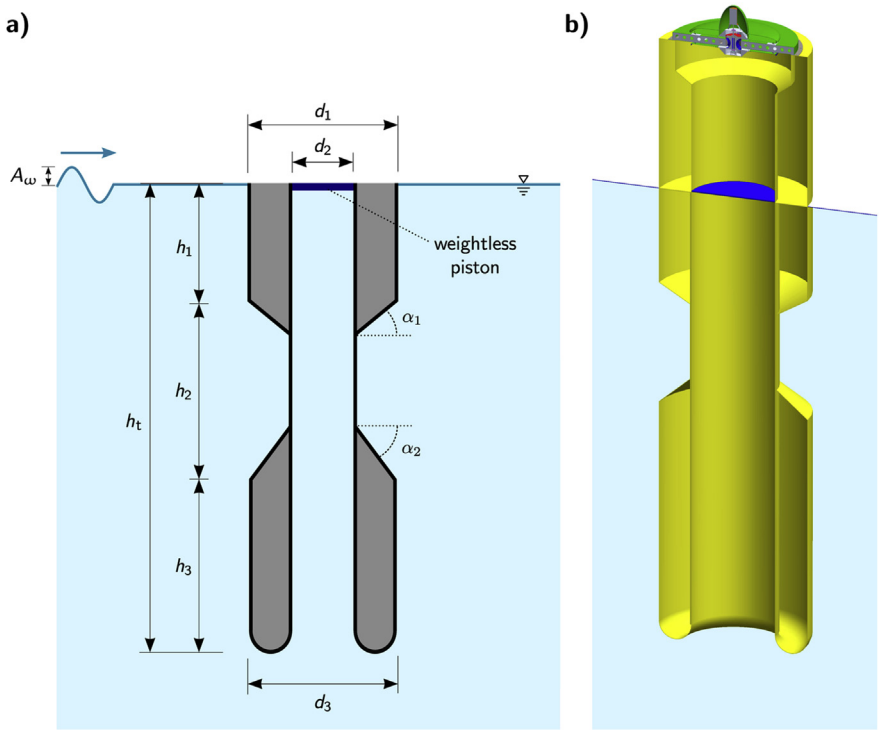

Fig. 7. a) Variables used in the spar-buoy OWC optimisation, from Ref. [19]. b) Three-dimensional view of the optimised spar-buoy OWC.

[28]. These performance indicators are directly related to system costs and also to system dynamics.

In general, it can be said that, for the same power output, the higher the velocity the lower the size and costs associated to the PTO. This is due to the fact that, for the same power output, the forces are inversely proportional to velocities. Furthermore, a structure designed to withstand lower levels of stresses, especially compressive, is expected to have smaller mass and lower cost. If the loads are cyclic, fatigue will aggravate the problems.

A performance indicator to assess the typical mean force on a WEC can be defined as

$$\Pi_F = \frac{\overline{P}_{\text{abs}}}{\overline{v}_{\text{PTO}}}, \tag{29}$$

where $\overline{P}_{\text{abs}}$ is the absorbed power by the PTO and v_{PTO} represents a typical velocity associated with the component of the PTO system with slowest motion. At an early stage of development it is unlikely to have a preliminary mechanical design of the WEC structure and, probably, this is the best indicator of the future relative costs of the PTO.

In the case of a turbine

$$\overline{P}_{\text{abs}} = \overline{P}_{\text{turb}}, \tag{30}$$

and

$$\overline{v}_{\text{PTO}} = \frac{\overline{\Omega}\, d}{2}, \tag{31}$$

from which it may be concluded that air turbines are subjected to lower forces than hydraulic systems, typically 100 times smaller, representing an advantage especially in terms of reliability. From the control perspective, hydraulic systems present more problems for optimizing the mean power output and also to control the excess of available energy in highly energetic sea states. These factors should be considered when assessing different types of wave energy technologies.

A performance indicator related to the annual absorbed energy per unit volume,

$$\Pi_{EV} = \frac{E_{\text{abs}}}{V_{\text{WEC}}}, \tag{32}$$

can give an indirect indication of the expected relative cost of energy. Here $E_{\text{abs}} = \overline{P}_{\text{abs}}\, t_{\text{year}}$ is the yearly absorbed energy, t_{year} is the operational time considered in one year and V_{WEC} is the submerged volume of the WEC. In a preliminary stage, where the mechanical design has not yet been performed, an effective cost indicator based on the submerged volume should be more reliable than a performance indicator based on the weight of the most expensive structural material used in the system.

For sinusoidal waves, the relation between the amplitude, A, and its root-mean-square (rms) is simply $A = \sqrt{2}\, A^{\text{rms}}$. A performance indicator for the relative averaged vertical buoy displacement can be defined by

$$\Pi_d = \frac{\sqrt{2}\, X_1^{\text{rms}}}{H_s}. \tag{33}$$

where

$$X_1^{\text{rms}} = \frac{1}{N}\, \sqrt{\mathbf{X}_1 \cdot \mathbf{X}_1}. \tag{34}$$

Here $\mathbf{X}_1$ is the resultant vector of the Fast Fourier Transform (FFT) of the vector storing the last N time-steps of the buoy displacement $\mathbf{x}_1$.

The performance indicator (33) is directly related to dynamic stresses to which the WEC structure and the moorings are subjected. In the case of OWC buoys for monitoring applications, the vertical oscillations may affect the accuracy of the data acquired by installed sensors. As a result, this effect can limit the choice of the buoy type for specific applications where the displacement is a constraint.

Another important remark is that all devices considered here are floating ones. If deployed at the same water depth, the mooring lines systems should have similar lengths and costs. Consequently, they have not been included in the analysis.

The performance indicators are used to compare devices after a detailed numerical simulation of each system. It is expected that any of the wave energy technologies that embarks in the way of commercialisation will be subject to a learning process, which would be translated into a reduction of costs. This evolution of costs can be represented through learning curves, as it has been done for other renewable energy technologies, *e.g.* photovoltaics and wind energy. However, at the current stages, it is considered sufficient, for the purpose of this study, to deal with the current picture of the technologies evaluated, all of them well inside the development process towards the demonstration at full scale.

5. Results

All the numerical results report to an Atlantic deployment site off the western coast of Portugal, characterized by a set of 14 sea-states as described in Table 1 [19].

5.1. Optimisation of the spar-buoy OWC

The spar-buoy OWC geometry is described in Fig. 7 a. For the hydrodynamic optimisation, the diameter, d_1, was set to 2.5 m; the draft was $l_{\text{turb}} = 7.5$ m; the angles α_1 and α_2 were set to 30° and 45°, respectively. The optimisation considered the diameters d_2 and d_3, and the lengths h_2 and h_3 as design variables. The optimised buoy is depicted in Fig. 7b. The submerged volume of the buoy is about 19.7 m^3.

The optimal turbine rotor diameter was selected according to the methodology presented in Section 4. In this procedure, the rotational speed was assumed not to be constrained by such factors as centrifugal stresses, occurrence of transonic flow or electrical generator limitations. The turbine power output for each sea state of the wave climate is plotted in Fig. 8, as function of the rotational speed, for two rotor diameters, $d = 0.20$ m and $d = 0.25$ m. From the plotted data, the turbine rotor diameter of $d = 0.25$ m was selected. The primary reason for the choice was the typical rotational speed, around 3000 rpm, and a turbine runaway speed less than 11000 rpm for the studied sea states, see Fig. 8b. The operating rotational speed of the turbine, around 3000 rpm, allows the use of a standard electrical generator with a slightly larger shaft diameter and more robust bearings.

The parameters a and b of (19) were determined by an exponential least-square fitting of maximum turbine power output for each sea state, n, as function of the rotational speed, $\Omega_{\text{opt},n}$. The fitting curves are plotted in Fig. 8a and b, for the two selected rotor diameters, $d = 0.20$ m and $d = 0.25$ m. Results in Fig. 8 show that the maximum turbine power output for each sea state follows very well the exponential fitting curve.

Experimental tests reveal that the biradial turbine is characterized by a dimensionless relationship between pressure head and flow rate approximately given by Ref. [37].

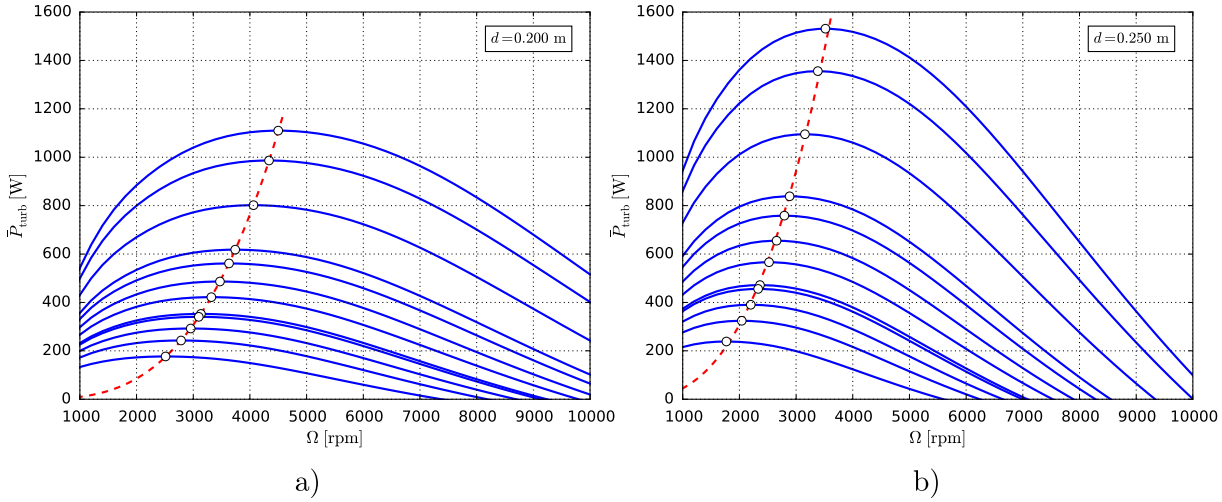

Fig. 8. Spar-buoy OWC time-averaged turbine power output, $\overline{P}_{\text{turb}}$, for each sea-state, n, of the considered wave climate, as function of the rotational speed, Ω, for turbine rotor diameters: a) $d = 0.20$ m and b) $d = 0.25$ m. The dots are maximum power output for each spectrum, $\Omega_{\text{opt},n}$. The broken line is the exponential curve that interpolates the maximum power output for each spectrum, $P_{\text{gen}}^{\text{opt}}$.

$$\Psi = K\,\Phi^{5/3}, \tag{35}$$

where K is a given constant, see Fig. 6a. By using (11) and (12) we get

$$p^* = \frac{\varrho_{\text{in}} K}{p_{\text{at}}}\, Q_{\text{turb}}^{5/3}\, \Omega^{1/3}\, d^{-3}, \tag{36}$$

where $Q_{\text{turb}} = \dot{m}_{\text{turb}}/\varrho_{\text{in}}$ is the volumetric flow rate. Since $p^* \propto d^{-3}$, the spar-buoy OWC hydrodynamics and the turbine power output are very sensitive to the turbine diameter, d, as can be found by comparing Fig. 8a and b.

The sensitivity of the electrical power output to the generator control law is depicted in Fig. 9. In this figure, there is a broad region of values a and b where close to maximum electrical power output can be achieved. From (36) we found that around the typical turbine operating point of 3000 rpm a change of a few hundred rpm in the rotational speed has a small effect on the buoys' hydrodynamic performance since $p^* \propto \Omega^{1/3}$. Consequently, the biradial turbine presents a rather flat power output response, as function of the rotational speed, close to the maximum power output value for each sea state. The low sensitivity of the electrical power output to the generator control law is an interesting feature of this PTO system.

Fig. 10 shows the effect of the turbine/generator set inertia in the annual-averaged turbine and electrical generator power outputs. As expected by the low sensitivity of the hydrodynamics to the turbine rotational speed, turbine and the electrical generator power outputs are not greatly affected by the inertia. The turbine power output decreases when the inertia increases as the turbine rotational speed is less sensitive to the variations in the instantaneous pneumatic power. Conversely, the electrical power output increases with the increase in inertia as the generator works with small turbine power fluctuations and, in average, it works at a higher load.

5.2. Optimisation of the coaxial-duct OWC

The coaxial-duct OWC was designed following the same methodology used for the spar-buoy OWC. The optimisation comprises the variables as described in Fig. 11a: the heights $h_1,\ldots,d_4$ and the diameter d_3. The diameters d_1 and d_2 were fixed during the optimisation procedure. For comparison with the spar-buoy OWC, the

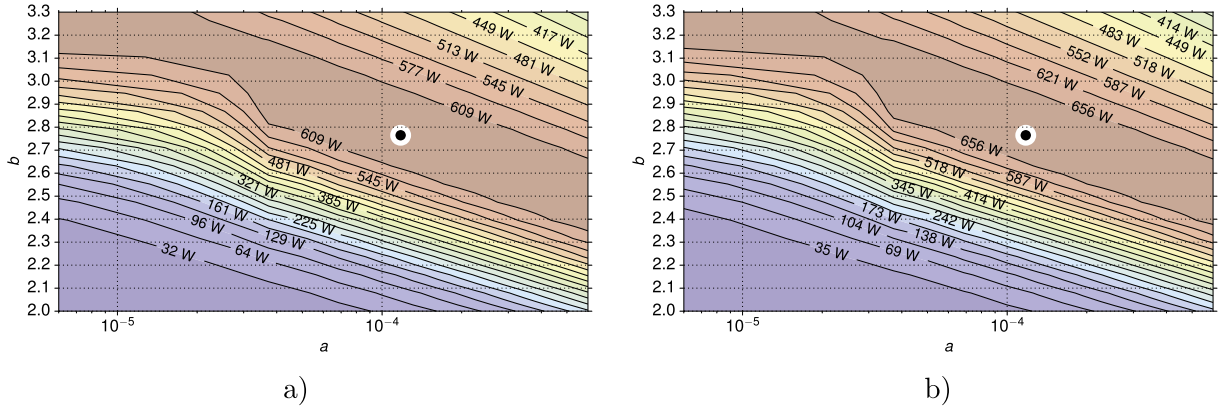

Fig. 9. Spar-buoy OWC annual-averaged electrical power output for the considered wave climate, $\overline{P}_{\text{elect}}$, as function of the constants a and b of the generator control law, Eq. (21), for two generator rated powers: a) $P_{\text{gen}}^{\text{rated}} = 1500$ W and b) $P_{\text{gen}}^{\text{rated}} = 3000$ W. The dots correspond to the optimal turbine values a and b of (19). The computations were performed for inertia $I = 0.1$ kg m^2.

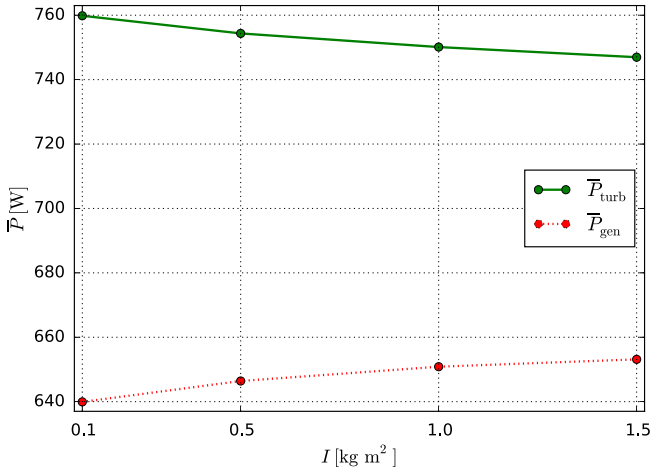

Fig. 10. Spar-buoy OWC annual-averaged turbine and electrical power outputs as functions of the inertia, I, considering a turbine rotor diameter of $d = 0.25$ m and a generator rated power of $P_{\text{gen}}^{\text{rated}} = 1500$ W.

outer diameter d_2 was also set to 2.5 m. The inner diameter d_1 was chosen to have equal cross-sectional areas for the inner duct and outer annular duct, $d_1 = d_2/\sqrt{2}$. This condition guarantees equal mean flow velocities in both ducts. A schematic representation of the optimised geometry is shown in Fig. 11. An optimal draft of 8.8 m was obtained resulting in a submerged volume of 8.1 m^3.

The parametric study of the air turbine rotor diameter is plotted in Fig 12, considering two turbine rotor diameters: $d = 0.20$ m and $d = 0.25$ m. From this plot, a turbine rotor diameter $d = 0.25$ m was selected. This is the smallest rotor diameter delivering an annual-averaged turbine power output close to 300 W. In Fig. 12 the exponential curve that fits the maximum turbine power output for each sea state is also plotted, from which constants a and b were computed for each rotor diameter.

Fig. 13 shows that the constants a and b can be used for the generator control law, as these point coordinates fall within the maximum electrical power output range.

The effect of the turbine/generator set inertia is depicted in Fig. 14. As with the spar-buoy OWC, the inertia has a minor effect on the electrical power conversion.

5.3. Comparison of the optimised buoys

The electrical power output follow, as expected, the pattern of the turbine power output as function of the significant wave height, H_s, and the energy period, T_e, of the spectra, see Figs. 15 and 16. Comparing the turbine and the generator power outputs it is clear that the generator efficiency has a strong impact on the system performance. As expected due to the small diameter of the buoys, the maximum power extraction occurs for the lower energy periods and the higher significant wave heights. It should be noted that these buoys do not operate in resonance conditions and, consequently, their efficiency is significantly lower than that of larger diameter buoys.

In terms of turbine and electrical output powers, the spar-buoy OWC outperforms the coaxial-duct OWC. However, for certain applications where the large buoy motion amplitude of the spar-buoy OWC may be inconvenient (possibly because of the installed sensors), the coaxial-duct OWC may constitute a valuable alternative, see Fig. 17.

All the depicted results in Figs. 15–17 should be considered as qualitative for the larger values of H_s. Under these high-amplitude motion conditions, the linear wave theory does not give accurate results.

The performance measures are shown in Table 2 for the spar-buoy OWC and the coaxial-duct OWC. For the two WECs, the annual-averaged electrical power output, $\overline{P}_{\text{elect}}$, complies with the minimum required value of 300 W. The mean electrical power is higher for the spar-buoy OWC, which means that it is able to absorb more energy for the considered characteristic diameter. The yearly absorbed energy per unit volume Π_{EV} is 285 kWh/m^3 for the spar-

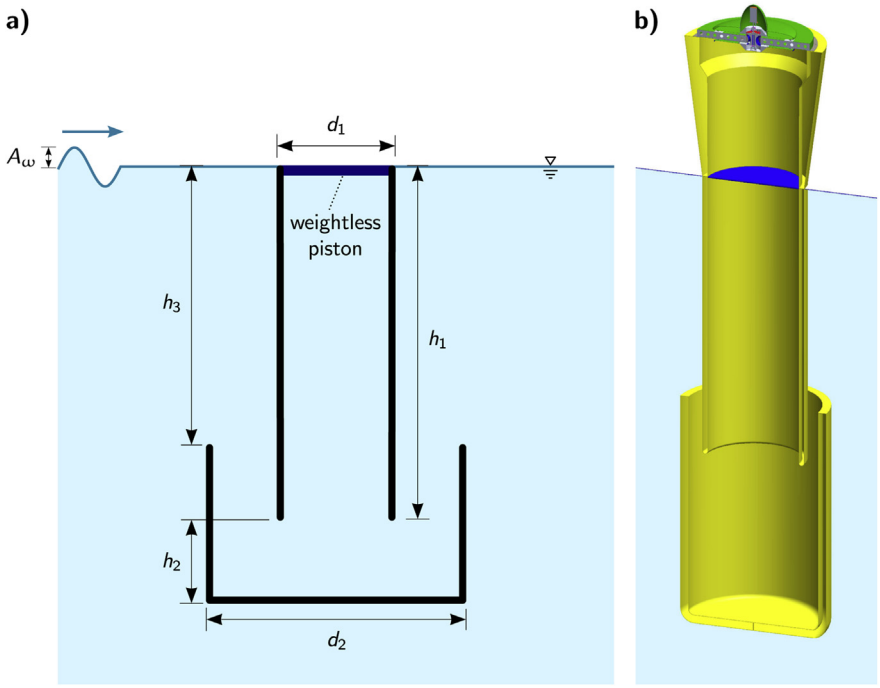

Fig. 11. a) Variables used in the optimisation of the coaxial-duct OWC b) Schematic representation of the optimised buoy.

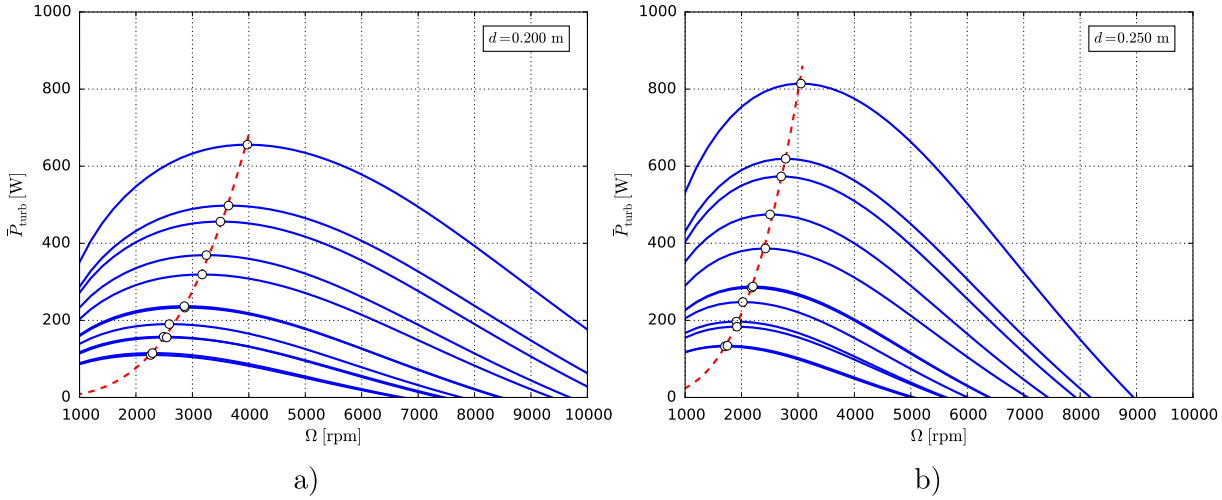

Fig. 12. Coaxial-duct OWC time-averaged turbine power output, $\overline{P}_{\text{turb}}$, for each sea-state, n, of the considered wave climate, as function of the rotational speed, Ω, for turbine rotor diameters: a) $d = 0.20$ m and b) $d = 0.25$ m. The dots are maximum power output for each spectrum, $\Omega_{\text{opt},n}$. The broken line is the exponential curve that interpolates the maximum power output for each spectrum, $P_{\text{gen}}^{\text{opt}}$.

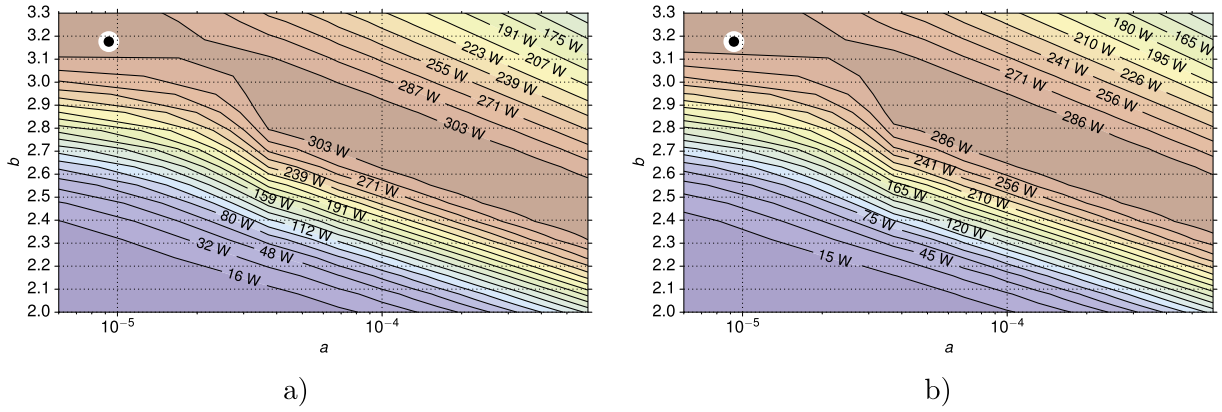

Fig. 13. Coaxial-duct OWC annual-averaged electrical power output for considered wave climate, $\overline{P}_{\text{elect}}$, as function of the constants a and b of the generator control law, Eq. (21), for two generator rated powers: a) $P_{\text{gen}}^{\text{rated}} = 1500$ W and b) $P_{\text{gen}}^{\text{rated}} = 3000$ W. The dots correspond to the optimal turbine values a and b of (19). The computations were performed for inertia $I = 0.1$ kg m^2.

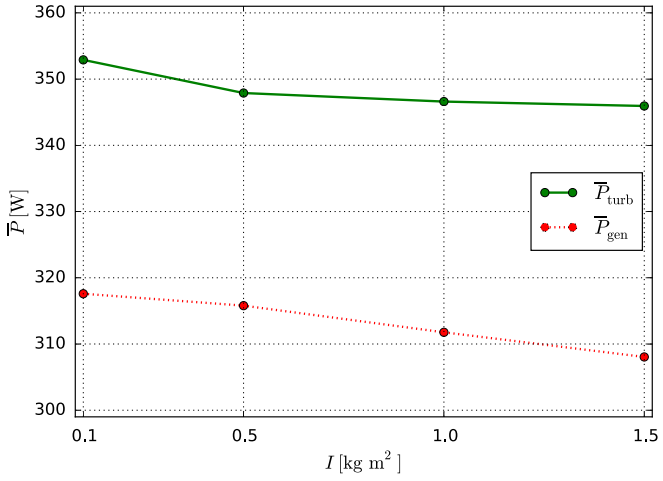

Fig. 14. Coaxial-duct OWC annual-averaged turbine and electrical power outputs as functions of the inertia, I, considering a turbine rotor diameter $d = 0.25$ m and a generator rated power of $P_{\text{gen}}^{\text{rated}} = 1500$ W.

buoy OWC and 343 kWh/m^3 for the coaxial-duct OWC, which indicates that the spar-buoy OWC is estimated to be structurally more expensive than the coaxial-duct OWC.

In what concerns the mean absorbed energy per unit linear velocity of the PTO, Π_F, the spar-buoy OWC presents the highest value. It is expected that a higher Π_F results in a more expensive PTO. It should be remarked that this performance indicator is more suited to compare different devices with similar power outputs, which is not the case of the spar-buoy OWC and the coaxial-duct OWC. Comparing the two types of buoys in term of volume, the coaxial-duct OWC should have a lower manufacturing cost. However, the consequences of the lower buoyancy of the coaxial-duct OWC should be analysed with caution specially for storm conditions.

In addition, the coaxial-duct OWC showed a displacement ratio of 0.295, while it is 1.103 for the spar-buoy OWC. This means that the expected displacements for the same wave climate can be 4 times higher for the spar-buoy OWC in comparison with the coaxial-duct OWC. The required specifications (especially in terms of allowed accelerations) of instruments to be installed on these oceanographic buoys might dictate which of these buoys are acceptable or not for the intended application.

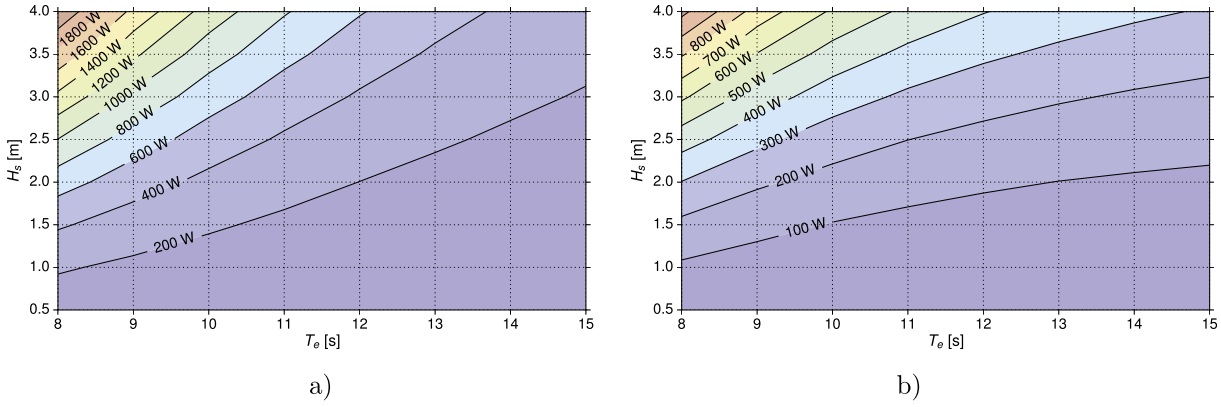

Fig. 15. Turbine power output as function of T_e and H_s for $I = 0.1$ kg m^2 and $P_{gen}^{rated} = 1500$ W. a) spar-buoy OWC and b) coaxial-duct OWC.

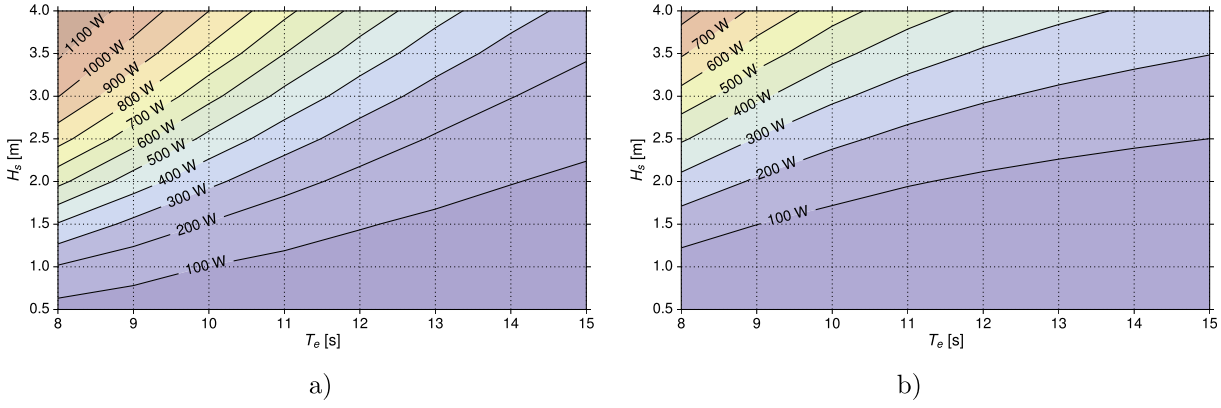

Fig. 16. Generator electrical power output as function of T_e and H_s for $I = 0.1$ kg m^2 and $P_{gen}^{rated} = 1500$ W. a) spar-buoy OWC and b) coaxial-duct OWC.

6. Conclusions

In the present paper, a systematic methodology is proposed for the design of wave energy converters. The methodology was splitted into two main processes: design and implementation. The design process was divided into three sub-processes: preliminary design, detailed design and model testing.

The detailed design of a spar-buoy OWC and a coaxial-ducted OWC for oceanographic monitoring applications was the main focus of the paper. This involved the buoy hydrodynamic optimisation (geometry) and power take-off sizing and selection. The methodology proposed for optimal sizing and selection of the turbine and the generator is simple and effective, and takes into account the wave climate of the deployment site. Both components of the power take-off system are tightly connected through a simple and effective control law of the generator electromagnetic torque. In the case of a biradial turbine, it is shown that the electrical power output has low sensitivity to a change in the generator control law parameters within a large region around the optimal values.

The performance assessment of both designs consisted in the computation of the scatter diagrams for the turbine power output,

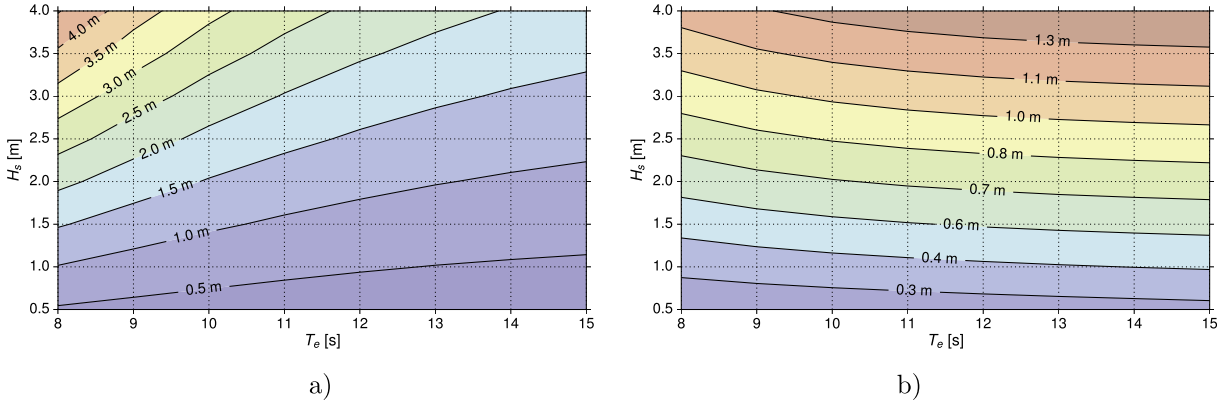

Fig. 17. Averaged vertical buoy motion amplitude, $\sqrt{2}X_1^{rms}$, as function of T_e and H_s for $I = 0.1$ kg m^2 and $P_{gen}^{rated} = 1500$ W. a) spar-buoy OWC and b) coaxial-duct OWC.

Table 2
Performance indicators for the optimised devices.

Performance indicator	Spar-buoy OWC	Coaxial-duct OWC	Units
$\overline{P}_{elect}$	640	318	[W]
Π_d	1.103	0.295	[−]
Π_{EV}	285	343	[kWh/m^3]
Π_F	18.47	10.53	[N]

electrical power output and root-mean-square of the buoy displacement, as well as the evaluation of a set of performance indicators. The performance indicators are well suited for broad estimation and a simple comparison of the possible costs associated with the WECs, especially at an initial phase of development. However, they should not be the only factors to be taken into account for assessing a wave energy technology. There are other considerations like construction costs, installation, O&M, decommissioning and environmental impact that should be analysed to make a complete and proper technology assessment.

The analysis carried out revealed that these self-powered sensor buoys are able to provide the required annual-averaged power output for the considered wave climate. The power absorption capacity of these small diameter buoys is rather low in comparison with the expected electrical power output of larger diameter buoys designed for electrical grid supply. Indeed, the objective of this self-powered sensor buoys is long-term monitoring of remote areas with minimal maintenance.

The research confirmed that floating WECs based on the OWC principle have a large potential and are attractive candidates for a next generation of self-powered oceanographic buoys aiming at long-term deployment.

Acknowledgements

The research was partially funded by the Portuguese Foundation for Science and Technology (FCT) through IDMEC, under LAETA Pest-OE/EME/LA0022. The first author was funded by FCT researcher grant No. IF/01457/2014. The second author was supported by the Marie Curie Actions of the European Union's Seventh Framework Programme FP7/2007-2013/ under REA grant agreement number 607656 (OceaNet project). The forth author was supported by post-doctoral fellowship SFRH/BPD/93209/2013 from FCT. This work has received funding from the European Union's Horizon 2020 research and innovation programme under grant agreement No 654444 (OPERA Project) and from the FCT project PTDC/MAR-TEC/0914/2014.

The authors would like to thank the anonymous reviewers for comments that helped to improve the manuscript.

References

[1] Lund H. Renewable energy strategies for sustainable development. Energy 2007;32(6):912–9.
[2] Lund H, Østergaard PA, Stadler I. Towards 100% renewable energy systems. Appl Energy 2011;88(2):419–21.
[3] EC, Innovation in the blue economy: realising the potential of our seas and oceans for jobs and growth., Available at: http://ec.europa.eu/maritimeaffairs/policy/index_pt.htm.
[4] Gouin J. Wave energy conversion systems designed for sensor buoys. Electro Standards Laboratories; 2008.
[5] Jerica N, Ertekin R Cengiz, Davis Edward P. In-ocean experiments of a wave energy conversion device when moored to an anchor and to a drogue. J Ocean Technol 2013;8(1):72–85.
[6] Chaffey M, Mellinger E, Paul W. Communications and power to the seafloor: MBARI's ocean observing system mooring concept. In: OCEANS, 2001. MTS/IEEE conference and exhibition, vol. 4; 2001. p. 2473–81. http://dx.doi.org/10.1109/OCEANS.2001.968389.
[7] Chaffey M, Bird L, Erickson J, Graybeal J, Hamilton A, Headley K, et al. MBARI's buoy based seafloor observatory design. In: OCEANS '04. MTTS/IEEE TECHNO-OCEAN '04, vol. 4; 2004. p. 1975–84. http://dx.doi.org/10.1109/OCEANS.2004.1406447.
[8] Monterey Bay Aquarium Research Institute. Harnessing the awesome power of the ocean waves, Available at: http://www.mbari.org/news/homepage/2012/powerbuoy/powerbuoy.html (accessed 21.11.15.).
[9] Monterey Bay Aquarium Research Institute. Experimental wave-power buoy survives winter in Monterey Bay, Available at: http://www.mbari.org/news/homepage/2015/powerbuoy/powerbuoy-update.html (accessed 21.11.15).
[10] Masuda Y. An experience with wave power generation through tests and improvement. In: Evans DV, Falcão AF de O, editors. IUTAM symp. Hydrodynamics of ocean-Wave energy utilisation. Springer-Verlag; 1986. p. 445–52.
[11] Falcão AFO, Gato LMC, Nunes EPAS. A novel radial self-rectifying air turbine for use in wave energy converters. Renew Energy 2013;50:289–98. http://dx.doi.org/10.1016/j.renene.2012.06.050.
[12] Masuda Y, McCormick ME. Experiences in pneumatic wave energy conversion in Japan. In: McCormick ME, Kim YC, editors. Proceeding of ASCE specialty conference on utilization of ocean waves-wave to energy conversion; 1986. p. 1–33.
[13] Torre-Enciso Y, Ortubia I, López de Aguileta LI, Marqués J. Mutriku wave power plant: from the thinking out to the reality. In: Proc 8th european wave tidal energy conf. Uppsala: Sweden; 2009. p. 319–29.
[14] Falcão AFO, Henriques JCC, Gato LMC. Air turbine optimization for a bottom-standing oscillating-water-column wave energy converter. J Ocean Eng Mar Energy 2016:1–14. http://dx.doi.org/10.1007/s40722-016-0045-7.
[15] Bocotti P. Comparison between a U-OWC and a conventional OWC. Ocean Eng 2007;34(5–6):799–805. http://dx.doi.org/10.1016/j.oceaneng.2006.04.005.
[16] Arena F, Romolo A, Malara G, Ascanelli A. On design and building of a U-OWC wave energy converter in the Mediterranean Sea. In: Proceedings of the 32nd international conference on ocean, offshore and arctic engineering, OMAE 2013, nantes, France; 2013.
[17] Takashi, T., Wave force utilizing power plant equipped with resonance sleeve, Japanese Patent JPS55151176 (A) (1980).
[18] Falcão AFO, Henriques JCC. Oscillating-water-column wave energy converters and air turbines: a review. Renew Energy 2016;85:1391–424. http://dx.doi.org/10.1016/j.renene.2015.07.086.
[19] Gomes RPF, Henriques JCC, Gato LMC, Falcão AFO. Hydrodynamic optimization of an axisymmetric floating oscillating water column for wave energy conversion. Renew Energy 2012;44:328–39. http://dx.doi.org/10.1016/j.renene.2012.01.105.
[20] Curran R, Gato LMC. The energy conversion performance of several types of Wells turbine designs. Proc Inst Mech Eng Part A J Power Energy 1997;211(2):133–45. http://dx.doi.org/10.1243/0957650971537051.
[21] Falcão AFO, Gato LMC. Air turbines. In: Sayigh A, editor. Comprehensive renewable energy. Ocean energy, vol. 8. Oxford: Elsevier; 2012. p. 111–49. http://dx.doi.org/10.1016/B978-0-08-087872-0.00805-2.
[22] Falcão AFO, Henriques JCC, Gato LMC, Gomes RPF. Air turbine choice and optimization for floating oscillating-water-column wave energy converter. Ocean Eng 2014;75:148–56. http://dx.doi.org/10.1016/j.oceaneng.2013.10.019.
[23] Falcão AF de O. Wave energy utilization: a review of the technologies. Renew Sustain Energy Rev 2010;14(3):899–918. http://dx.doi.org/10.1016/j.rser.2009.11.003.
[24] Heath TV. A review of oscillating water columns, Philosophical Transactions of the Royal Society of London A: mathematical. Phys Eng Sci 2011;370(1959):235–45. http://dx.doi.org/10.1098/rsta.2011.0164.
[25] Würfel P. Physics of solar cells: from principles to new concepts. second ed. Wiley-VCH Verlag GmbH; 2009.
[26] Zhang X, Zhao L-D. Thermoelectric materials: energy conversion between heat and electricity. J Materiomics 2015;1(2):92–105.
[27] Zhu T, Ertekin E. Phonon transport on two-dimensional graphene/boron nitride superlattices. Phys Rev B 2014;90(19):195209.
[28] Babarit A, Hals J, Muliawan M, Kurniawan A, Moan T, Krokstad J. Numerical benchmarking study of a selection of wave energy converters. Renew Energy 2012;41:44–63. http://dx.doi.org/10.1016/j.renene.2011.10.002.
[29] PMI Guía. De los fundamentos para la dirección de proyectos. Pennsylvania, USA: Project Management Institute, Inc; 2008.
[30] Ruellan M, BenAhmed H, Multon B, Josset C, Babarit A, Clement A. Design methodology for a SEAREV wave energy converter. IEEE Trans Energy Convers 2010;25(3):760–7. http://dx.doi.org/10.1109/TEC.2010.2046808.
[31] Dally WR, Brown CA. A modeling investigation of the breaking wave roller with application to cross-shore currents. J Geophys Res Oceans 1995;100(C12):24873–83. http://dx.doi.org/10.1029/95JC02868.
[32] Yemm R, Pizer D, Retzler C, Henderson R. Pelamis: experience from concept to connection, Philosophical Transactions of the Royal Society of London A: mathematical. Phys Eng Sci 2011;370(1959):365–80. http://dx.doi.org/10.1098/rsta.2011.0312.
[33] Dalton GJ, Alcorn R, Lewis T. Case study feasibility analysis of the Pelamis wave energy convertor in Ireland. Portugal N. Am Renew Energy 2010;35(2):443–55. http://dx.doi.org/10.1016/j.renene.2009.07.003.
[34] Kofoed JP, Frigaard P, Friis-Madsen E, Sørensen HC. Prototype testing of the wave energy converter Wave Dragon. Renew Energy 2006;31(2):181–9. http://dx.doi.org/10.1016/j.renene.2005.09.005.
[35] Weber J. WEC technology readiness and performance matrix - finding the best research technology development trajectory. In: Proc. of the 4th International Conference on Ocean Energy, ICOE'12, dublin, dublin, Ireland; 2012.

[36] Mankins JC. Technology readiness levels: a white paper. NASA; 1995. available online at: http://www.hq.nasa.gov/office/codeq/trl/trl.pdf (Last accessed date 05.05.16.).
[37] Falcão AFO, Gato LMC, Nunes EPAS. A novel radial self-rectifying air turbine for use in wave energy converters. Part 2. Results from model testing. Renew Energy 2013;53:159–64. http://dx.doi.org/10.1016/j.renene.2012.11.018.
[38] Henriques JCC, Gomes RPF, Gato LMC, Falcão AFO, Robles E, Ceballos S. Testing and control of a power take-off system for an oscillating-water-column wave energy converter. Renew Energy 2016;85:714–24. http://dx.doi.org/10.1016/j.renene.2015.07.015.
[39] Gomes RPF, Henriques JCC. Experimental validation of a spar-buoy design for wave energy conversion. available online at:. 2013. http://www.fp7-marinet.eu/public/docs/SPAR_BUOY_WEC_Access_Period1.pdf (Last accessed date 05.05.16.).
[40] Fonseca F, Gomes RPF, Henriques JCC. Dynamics of oscillating water column spar-buoy wave energy converters deployed in array and its survivability in extreme conditions. available online at:. 2015. http://www.fp7-marinet.eu/public/docs/MARINET%20TA1%20-%20SPAR-BUOY%20ARRAY%20V09.pdf (Last accessed date 05.05.16.).
[41] Goda Y. Random seas and design of maritime structures. second ed. Singapure: World Scientific Publishing; 2000.
[42] Henriques JCC, Lopes MFP, Gomes RPF, Gato LMC, Falcão AFO. On the annual wave energy absorption by two-body heaving WECs with latching control. Renew Energy 2012;45:31–40. http://dx.doi.org/10.1016/j.renene.2012.01.102.
[43] Newman JN, Lee CH. WAMIT user manual. available online at:. 2004. http://www.wamit.com/manual.htm (Last accessed date 22.11.15.).
[44] Lee CH, Newman JN. Computation of wave effects using the panel method. In: Chakrabarti SK, editor. Numerical models in fluid-structure interaction. Southampton: WIT Press; 2004.
[45] Keesman KJ. System identification, an introduction. London: Springer-Verlag; 2011. http://dx.doi.org/10.1007/978-0-85729-522-4.
[46] Perez T, Fossen TI. A Matlab toolbox for parametric identification of radiation-force models of ships and offshore structures. Model Identif Control 2009;30(1):1–15. http://dx.doi.org/10.4173/mic.2009.1.1.
[47] Henriques JCC, Gato LMC, Falcão AFO, Robles E, Faÿ F-X. Latching control of a floating oscillating-water-column wave energy converter. Renew Energy 2016;90:229–41. http://dx.doi.org/10.1016/j.renene.2015.12.065.
[48] Henriques JCC, Gato LMC, Lemos JM, Gomes RPF, Falcão AFO. Peak-power control of a grid-integrated oscillating water column wave energy converter. Energy 2016;109:378–90. http://dx.doi.org/10.1016/j.energy.2016.04.098.
[49] Dixon SL, Hall CA. Fluid mechanics and thermodynamics of turbomachinery. seventh ed. Oxford: Butterworth-Heinemann; 2013.
[50] Dick E. In: Fundamentals of turbomachines of fluid mechanics and its applications, vol. 109. Netherlands: Springer; 2015. http://dx.doi.org/10.1007/978-94-017-9627-9.
[51] Tedeschi E, Carraro M, Molinas M, Mattavelli P. Effect of control strategies and power take-off efficiency on the power capture from sea waves. Energy Convers IEEE Trans 2011;26(4):1088–98. http://dx.doi.org/10.1109/TEC.2011.2164798.
[52] Justino PAP, Falcão AF de O. Rotational speed control of an OWC wave power plant. J Offshore Mech Artic Eng 1999;121(2):65–70. http://dx.doi.org/10.1115/1.2830079.
[53] Henriques JCC, Falcão AFO, Gomes RPF, Gato LMC. Air turbine and primary converter matching in spar-buoy oscillating water column wave energy device. In: Proceedings of the 32nd International Conference on Ocean, Offshore and Arctic Engineering, omae 2013, nantes, France; 2013.
[54] de O. Falcão AF. Control of an oscillating-water-column wave power plant for maximum energy production. Appl Ocean Res 2002;24(2):73–82. http://dx.doi.org/10.1016/S0141-1187(02)00021-4.
[55] Demirtas O. Evaluating the best renewable energy technology for sustainable energy planning. Int J Energy Econ Policy 2013;3:23–33.